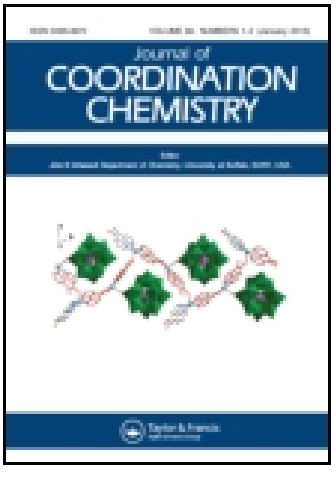

Journal of Coordination Chemistry
Publication details, including instructions for authors and subscription information:
http://www.tandfonline.com/loi/gcoo20

Di-, tri-, and tetranuclear cobalt, copper, and manganese complexes bridged by μ-hydroxyl groups of tetradentate Schiff base ligands: structures, magnetic properties, and antitumor activities

Mei-Ju Niu[a], Da-Wei Sun[a], Huan-Huan Li[a], Zhi-Qiang Cao[a], Su-Na Wang[a] & Jian-Min Dou[a]

[a] Shandong Provincial Key Laboratory of Chemical Energy Storage and Novel Cell Technology, School of Chemistry and Chemical Engineering, Liaocheng University, Liaocheng, PR China

Accepted author version posted online: 10 Jan 2014.Published online: 30 Jan 2014.

To cite this article: Mei-Ju Niu, Da-Wei Sun, Huan-Huan Li, Zhi-Qiang Cao, Su-Na Wang & Jian-Min Dou (2014) Di-, tri-, and tetranuclear cobalt, copper, and manganese complexes bridged by μ-hydroxyl groups of tetradentate Schiff base ligands: structures, magnetic properties, and antitumor activities, Journal of Coordination Chemistry, 67:1, 81-95, DOI: 10.1080/00958972.2013.876625

To link to this article: http://dx.doi.org/10.1080/00958972.2013.876625

Journal of Coordination Chemistry, 2014
Vol. 67, No. 1, 81–95, http://dx.doi.org/10.1080/00958972.2013.876625

Di-, tri-, and tetranuclear cobalt, copper, and manganese complexes bridged by μ-hydroxyl groups of tetradentate Schiff base ligands: structures, magnetic properties, and antitumor activities

MEI-JU NIU*, DA-WEI SUN, HUAN-HUAN LI, ZHI-QIANG CAO, SU-NA WANG and JIAN-MIN DOU

Shandong Provincial Key Laboratory of Chemical Energy Storage and Novel Cell Technology, School of Chemistry and Chemical Engineering, Liaocheng University, Liaocheng, PR China

(*Received 26 March 2013; accepted 20 November 2013*)

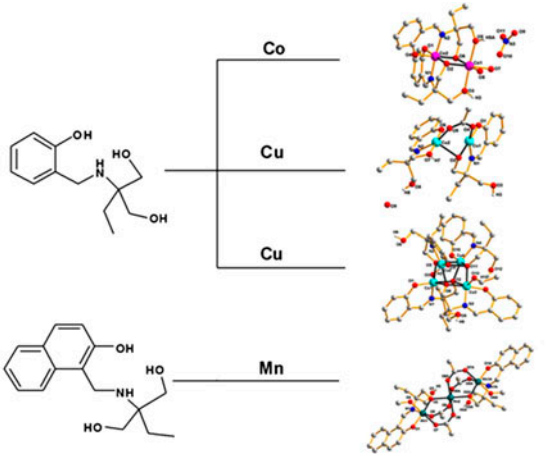

$[Co_2(HL^1)_2(H_2O)_2](NO_3)$ (**1**), $[Cu_2(H_2L^1)(HL^1)(CH_3COO)]\cdot H_2O$ (**2**), $[Cu_4(HL^1)_4(C_2H_5OH)]\cdot C_2H_5OH\cdot H_2O$ (**3**), and $[Mn_3(HL^2)_2(CH_3OH)_2(CH_3COO)_4]\cdot 2(CH_3OH)\cdot H_2O$ (**4**) {$\mathbf{H_3L^1}$ = 2-ethyl-2-(2-hydroxybenzylideneamino)propane-1,3-diol, $\mathbf{H_3L^2}$ = 2-ethyl-2-[(2-hydroxynaphthalene-1-yl)methyleneamino]propane-1,3-diol} have been synthesized and characterized by IR spectra, elemental analyses, single-crystal X-ray diffraction, TGA, XRD, and magnetic measurements. Compound **1** possesses mixed-valence dinuclear $\{Co_2(\mu_2\text{-}O)_2\}$ with Co(II) and Co(III) ions linked through μ_2-hydroxyl of Schiff base ligands. Compound **2** displays a binuclear structure with $\{Cu_2(\mu_2\text{-}O)(\eta^2\text{-}COO)\}$ containing one μ_2-hydroxyl and a single *syn–syn* acetate bridge. Compound **3** is tetranuclear with a cube-shaped $\{Cu_4(\mu_3\text{-}O)_4\}$ core constructed by four Cu(II) centers and four μ_3-hydroxyls of Schiff base ligands. Compound **4** displays a linear trinuclear $\{Mn_3(\mu_2\text{-}O)_2(\eta^2\text{-}COO)_2\}$ structure in which the terminal Mn(III) and the central Mn(II) ions are linked by a μ_2-hydroxyl of Schiff base and two *syn–syn* acetate bridges. The results show that terminal hydroxyl groups of Schiff base ligands play an important role in assembling polynuclear compounds. Magnetic properties and

*Corresponding author. Email: niumeiju@163.com

antitumor activities of these compounds were investigated. The antitumor activities reveal that **1** and **2** are more effective antitumor agents for K-562 and HL-60, respectively.

Keywords: Schiff base; Polynuclear compounds; Hydroxyl group; Magnetic properties; Antitumor activities

1. Introduction

Synthesis of transition metal polynuclear compounds deserve special attention because of fascinating structural diversities in metal-organic frameworks and wide applications in catalysis [1], molecular magnetism [2], luminescence [3], heterogeneous catalysts [4], biological activities [5], etc. Such polynuclear metal compounds can be obtained using multidentate ligands, which often contain hydroxo and phenoxo donors. These specific structures could facilitate the formation of multinuclear metal compounds with new architectures bridged by hydroxo or phenoxo [6–10]. These OH-rich moieties have previously been used in the assembly of tetranuclear copper, nickel, and manganese cube complexes, and mixed-valence pentanuclear cobalt, double-cubane clusters [11, 12], etc. However, it is still a challenge to rationally design and control the coordination mode of ligands to afford various nuclearities.

To study the coordination behavior of these ligands with transition metals, we explore two OH-rich chelating Schiff bases, 2-ethyl-2-(2-hydroxybenzylideneamino)propane-1,3-diol ($\mathbf{H_3L^1}$) and 2-ethyl-2-((2-hydroxynaphthalene-1-yl)methyleneamino)propane-1,3-diol ($\mathbf{H_3L^2}$). Both ligands contain a tetradentate {NO3} donor set and a flexible hydroxyl moiety that possess chelating and bridging capabilities. The four potential donor sites and various coordination modes allow the ligands to synthesize new multinuclear compounds. We present the synthesis and structure of $[Co_2(HL^1)_2(H_2O)_2](NO_3)$ (**1**), $[Cu_2(H_2L^1)(HL^1)(CH_3COO)]\cdot H_2O$ (**2**), $[Cu_4(HL^1)_4(C_2H_5OH)]\cdot C_2H_5OH\cdot H_2O$ (**3**), and $Mn_3(HL^2)_2(CH_3OH)_2(CH_3COO)_4]\cdot 2(CH_3OH)\cdot H_2O$ (**4**). Single-crystal X-ray diffraction results show that the terminal hydroxyl moieties freely twist and bend to bridge or chelate metals, yielding compounds with different nuclearities. The magnetic properties and antitumor activities of the compounds have also been discussed.

2. Experimental

2.1. *General procedures and materials*

All reagents and solvents were commercially available and used without purification. The ligands were synthesized as described [13–15] and are given in scheme 1. $\mathbf{H_3L^1}$ and $\mathbf{H_3L^2}$ were obtained by condensation of salicylaldehyde or 2-hydroxy-1-naphthaldehyde with 2-amino-2-ethyl-1,3-propanediol in a 1 : 1 M ratio in methanol. We previously reported $\mathbf{H_3L^2}$ [16].

CAUTION: Perchlorate salts are potentially explosive and should be handled in small quantities.

$\mathbf{H_3L^1}$: Yield: 87%. m.p.: 94–96 °C. Selected IR (KBr pellet: cm^{-1}): 3444(s, ν_{O-H}), 1644(s, $\nu_{C=N}$), 1210(w, ν_{Ph-O}). ^1H NMR data (400 MHz, $CDCl_3$) δ/ppm 8.510(s, 1H, –C**H**=N), 7.920–6.753(m, 4H, AR–**H**), 3.920–3.631(t, 4H, –C**H**$_2$OH), 1.490–1.434(m, 2H, –C**H**$_2$CH$_3$), 0.902–0.854(t, 3H, –C**H**$_3$); ^{13}C NMR ($CDCl_3$): δ/ppm 164.829(1C, –**C**H=N), 163.792(1C, AR–OH), 133.216, 132.229, 126.658, 122.563, 116.354(5C, –**C**$_6$H$_4$), 66.300(2C, –**C**H$_2$OH), 65.386(1C, *tert*-C), 25.972(1C, –**C**H$_2$CH$_3$), 7.362(–CH$_2$**C**H$_3$). Anal. Calcd (%) for $C_{12}H_{17}NO_3$ (Mw, 223.27): C, 64.55; H, 7.67; N, 6.27%. Found: C, 64.31; H, 7.49; N, 6.39%.

2.2. *Syntheses*

2.2.1. Synthesis of $[Co_2(HL^1)_2(H_2O)_2](NO_3)$ (1). A methanol solution (10 mL) of $Co(NO_3)_2{\cdot}6H_2O$ (0.2911 g, 1 mM) was added dropwise to a stirring methanol solution (10 mL) containing $\mathbf{H_3L^1}$ (0.2233 g, 1 mM). After the addition of tetraethyl ammonium hydroxide aqueous solution (20%, about 1 mL), the mixture was stirred at room temperature for 4 h and then filtered. Brown crystals suitable for X-ray data collection were obtained by slow evaporation of methanol solution for one week.

Yield: 68%. m.p.: 343–346 °C. Selected IR (KBr pellet: cm^{-1}): 3433(s, ν_{O-H}), 1637(m, $\nu_{C=N}$), 1382, 859(m, ν_{NO3}) [17], 1195(m, ν_{Ph-O}), 623(m, ν_{Co-N}), 509(m, ν_{Co-O}), 474(m, ν_{Co-O}) [18]. Anal. Calcd (%) for $C_{24}H_{34}Co_2N_3O_{11}$ (Mw, 658.41): C, 43.78; H, 5.21; N, 6.38%. Found: C, 43.89; H, 4.91; N, 6.59%.

The synthetic procedures for other compounds were very similar to **1** and are discussed below.

2.2.2. Synthesis of $[Cu_2(H_2L^1)(HL^1)(CH_3COO)]{\cdot}H_2O$ (2). Tetraethyl ammonium hydroxide aqueous solution (20%, about 1 mL) was added to methanol solution of $Cu(CH_3COO)_2{\cdot}H_2O$ (0.1996 g, 1 mM) and $\mathbf{H_3L^1}$ (0.2233 g, 1 mM). The mixture was stirred at room temperature for 4 h and then filtered. Green crystals suitable for X-ray data collection were obtained by slow evaporation of methanol solution for one week.

Yield: 78%. m.p.: 273–276 °C. Selected IR (KBr pellet, cm^{-1}): 3513(s, ν_{O-H}), 1627(s, $\nu_{C=N}$), 1570(vs νas_{COO-}), 1445(s, νs_{COO-}), 587(m, ν_{Cu-N}), 461(m, ν_{Cu-O}). Anal. Calcd (%) for $C_{26}H_{36}Cu_2N_2O_9$ (Mw, 647.65): C, 48.22; H, 5.60; N, 4.32. Found: C, 48.36; H, 5.45; N, 4.21.

2.2.3. Synthesis of $[Cu_4(HL^1)_4(C_2H_5OH)]{\cdot}C_2H_5OH{\cdot}H_2O$ (3). Tetraethyl ammonium hydroxide aqueous solution (20%, about 1 mL) was added to ethanol solution of $Cu(ClO_4)_2{\cdot}6H_2O$ (0.3705 g, 1 mM) and $\mathbf{H_3L^1}$ (0.2233 g, 1 mM). The mixture was stirred at room temperature for 4 h and then filtered. Green crystals suitable for X-ray data collection were obtained by slow evaporation of ethanol solution for one week.

Yield: 66%. m.p.: 255–258 °C. Selected IR (KBr pellet: cm^{-1}): 3447(s, ν_{O-H}), 1624(s, $\nu_{C=N}$), 586(m, ν_{Cu-N}), 469(m, ν_{Cu-O}). Anal. Calcd (%) for $C_{52}H_{74}Cu_4N_4O_{15}$ (Mw, 1249.36): C, 49.99; H, 5.97; N, 4.48%. Found: C, 50.45; H, 5.63; N, 4.82%.

2.2.4. Synthesis of $[Mn_3(HL^2)_2(CH_3OH)_2(CH_3COO)_4]{\cdot}2(CH_3OH){\cdot}H_2O$ (4). Tetraethyl ammonium hydroxide aqueous solution (20%, about 1 mL) was added to methanol solution of $Mn(CH_3COO)_2{\cdot}4H_2O$ (0.2451 g, 1 mM) and $\mathbf{H_3L^2}$ (0.2733 g, 1 mM). The mixture was stirred at room temperature for 4 h and then filtered. Dark brown crystals were obtained from the solution for one week.

Yield: 72%. m.p.: 263–265 °C. Selected IR (KBr pellet: cm^{-1}): 3435(s, ν_{O-H}), 1621(s, $\nu_{C=N}$), 1540 (s, νs_{COO-}), 1384(s, νas_{COO-}), 1216(m, ν_{Ph-O}), 588(m, ν_{Mn-N}), 470(m, ν_{Mn-O}). Anal. Calcd (%) for $C_{46}H_{74}Mn_3N_2O_{22}$ (Mw, 1171.89): C, 47.15; H, 6.36; N, 2.39%. Found: C, 47.56; H, 6.69; N, 2.12%.

2.3. *Physical measurements*

IR spectra in KBr pellets (4000–400 cm^{-1}) were recorded on a Nicolet-5700 FT-IR spectrophotometer. Elemental analyses for C, H, and N were performed on a Perkin-Elmer 2400-II microanalysis instrument. ^{1}H and ^{13}C NMR spectra were obtained on a Varian Mercury Plus 400 MHz NMR spectrometer. Chemical shifts are reported in ppm with respect to the references and are stated relative to external tetramethylsilane for ^{1}H and ^{13}C NMR. Variable temperature susceptibility measurements were carried out with a SQUID MPMS XL7 magnetometer from 2.0 to 300 K at a magnetic field of 1 kOe. The molar susceptibility was corrected from the sample holder and the diamagnetic contributions of all constituent atoms using Pascal's constants.

2.4. *X-ray crystallography*

Suitable single crystals of **1–4** were mounted in glass capillaries and intensity data were measured on a Siemens Smart CCD diffractometer using graphite-monochromated Mo Kα radiation ($\lambda = 0.71073$ Å) at 298 K. Semi-empirical absorption corrections (multiscan) were applied with SADABS [19]. The structures were solved by direct methods and refined by full-matrix least-squares on F_o^2 with SHELXS-97 and SHELXL-97 [19]. Non-hydrogen atoms were refined anisotropically. Hydrogens were included in calculated positions and refined with isotropic thermal parameters riding on those of the parent atoms.

2.5. *Anticancer activities*

The anticancer activities of the compounds were studied using MTT assay [20] based on the cleavage of the yellow tetrazolium salt MTT [3-(4,5-dimethylthiazol-2-yl)-2,5-diphenyltetrazoliumbromide] to purple formazan crystals by metabolically active cells that could be quantified at 570 nm in DMSO. Cell lines of K-562 (human chronic neutrophilic leukemia) and HL-60 (human promyelocytic leukemia) were seeded in 96-well culture plates in RPMI-1640 medium containing 10% FBS and 1% antibiotics, maintained at 37 °C, 5% CO_2 in the CO_2 incubator for 24 h. Various concentrations of compounds dissolved in CH_3OH were added to the cells and incubation was continued for 48 h. After treatment, MTT was dissolved in the medium and added to each well, and then incubated for an additional 4 h. Following the removal of volatile materials, 100 μL of DMSO was added to dissolve the crystals. A reading was taken on a plate reader and absorbance was measured at 570 nm. Activities of compounds were measured as the percentage ratio of the absorbance of the treated cells to the untreated controls. The IC_{50} values were determined by non-linear regression analysis.

3. Results and discussion

3.1. *Syntheses*

The polynuclear compounds **1–4** have been prepared by simple reactions which involve the ligand in polar solvent, followed by complexation with the corresponding metal salt at room temperature with constant stirring. During the reaction, tetraethyl ammonium hydroxide is

added to deprotonate the ligands. The ligands are deprotonated at different levels and bound to the metal center either tri- or tetradentate.

3.2. *Descriptions of structures*

The crystallographic data, selected bond lengths and angles, and hydrogen bonding geometries are listed in tables 1–3. The supramolecular structures from hydrogen bonding interactions are listed in Supplementary material (figures S1–S4, see online supplemental material at http://dx.doi.org/10.1080/00958972.2013.876625).

3.2.1. Structure of $[Co_2(HL^1)_2(H_2O)_2](NO_3)$ (1). X-ray diffraction indicated that **1** crystallizes in the orthorhombic *Pna2₁* space group containing a $[Co_2(HL^1)_2]^+$ and a NO_3^- per asymmetric unit (figure 1). Two crystallographically independent cobalts are six-coordinate with tetragonal bipyramidal coordination geometries. For Co(1), four O(2), O(3), O(5), and O(6) of two deprotonated HL_1^{2-} and two aqua O(7) and O(8) form the coordination sphere with the two waters at apical positions. The equatorial plane of Co(2) is composed of two phenolic oxygens (O(1) and O(4)) and two terminal hydroxyl oxygens (O(2) and O(6)) of two $(HL^1)^{2-}$. The axial positions are occupied by two nitrogens of a different $(HL^1)^{2-}$. Co–O and Co–N bonds are 1.892(4)–2.092(4) Å. Co–O bonds in the square plane are 2.027–2.093 Å, while the Co–O and Co–N distances along the apical positions (2.109–2.146 Å) are elongated due to the Jahn–Teller effect [21]. The oxidation states of Co(1) and Co(2) could be identified as +2 and +3, respectively, consistent with the overall charge balance of the system [16] and the magnetic measurements [22]. The Schiff base is incompletely deprotonated and μ_2-$\eta^1:\eta^1:\eta^2:\eta^1$ connecting Co(1) and Co(2) ions (scheme 2a), forming a dinuclear $Co_2(\mu_2\text{-}O)_2$ core with the Co···Co distance of 2.963(12) Å. The Co–O–Co angles are 98.14(16)° and 96.99(16)°.

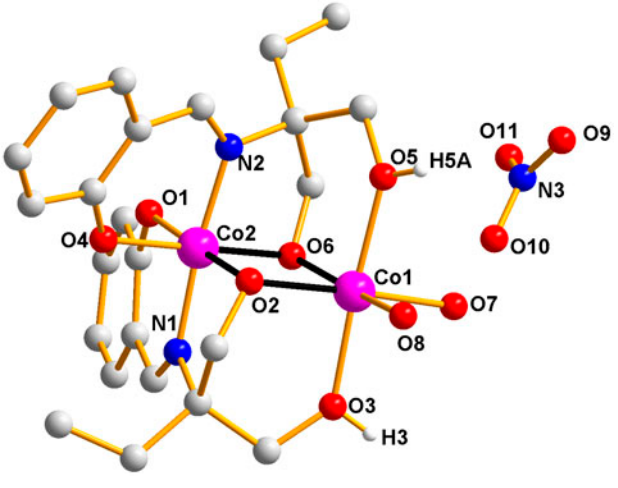

Figure 1. View of the molecular structure of **1**. For clarity, only the hydrogens on hydroxyl of Schiff base ligands are shown. Other hydrogens are omitted. The dinuclear unit is highlighted with black bonds. Co, purple; O, red; N, blue; C, gray; H, white (see http://dx.doi.org/10.1080/00958972.2013.876625 for color version).

Neighboring binuclear species in the crystal lattice are linked by intermolecular O(7)–H(7B)···O(4) hydrogen bonds into a 1-D zigzag chain structure. Adjacent chains are further linked by NO_3^- through O(7)–H(7C)···O(10) and O(5)–H(5A)···O(11) hydrogen bonding interactions into a 3-D hydrogen-bonded network (figure S1).

3.2.2. Structure of $[Cu_2(H_2L^1)(HL^1)\cdot(CH_3COO)]\cdot H_2O$ (2). Compound **2** is a dinuclear copper complex. The asymmetric unit contains two geometrically distinct copper centers, two Schiff base ligands, one acetate, and one free water (figure 2). The Cu(1) center is four-coordinate by imine N(1), phenolic oxygen O(1), and hydroxyl oxygen O(2) of one $(HL_1)^{2-}$, as well as acetate O(4), forming a slightly distorted square-planar coordination. Cu(1) is displaced by 0.134(2) Å from the least-square plane defined by the four donors with a mean deviation from the plane of 0.166(2) Å. Cu(2) has a distorted square-pyramidal geometry with $\tau = 0.287$ [trigonality index $\tau = (\beta-\alpha)/60$, where β and α are the two largest ligand–metal–ligand angles; $\tau = 0$ and 1 for the perfect square-pyramidal and trigonal-bipyramidal geometries, respectively [23]]. The basal plane is occupied by O(6), N(2), and O(7) of the other $(H_2L_1)^-$ and one O(5) of acetate; the apical position is occupied by phenolic O(2). The apical Cu(2)–O(2) bond length is longer than the corresponding ones in the basal plane, slightly elongated due to the Jahn–Teller effect of Cu with a d^9 configuration [8]. Cu(2) deviates 0.205(2) Å from the basal plane and the mean deviation of the donors from the basal plane is 0.612(2) Å.

For charge balance, the two crystallographically independent Schiff base ligands should be incompletely deprotonated $(HL^1)^{2-}$ and $(H_2L^1)^-$, respectively. Considering the strong O–H···O hydrogen interactions between the coordinated hydroxyl O(7) and O(2) of two different Schiff base ligands, the ligand with O7 should be assigned to be protonated with H on O7 (table 2). The ligands adopt μ_2-$\eta^1:\eta^1:\eta^2:\eta^0$ and μ-$\eta^1:\eta^1:\eta^1:\eta^0$ coordination modes [scheme 2(b) and (c)], respectively, connecting two coppers together with *syn–syn* bidentate acetate to form a $Cu_2(\mu_2\text{-O})(\mu\text{-COO})$ core. The Cu(1)···Cu(2) distance and the

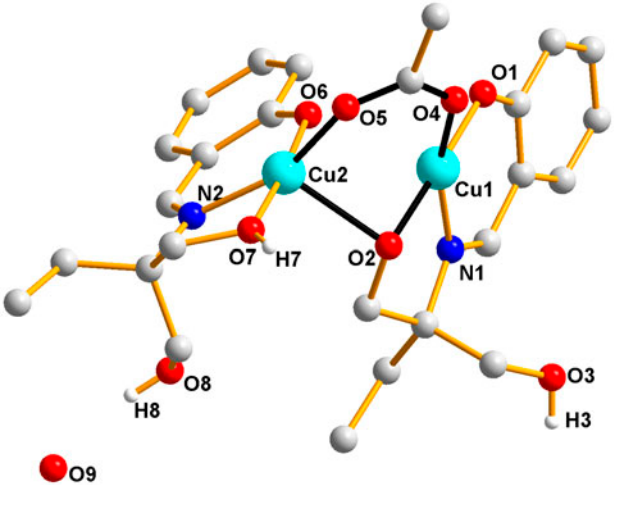

Figure 2. View of the molecular structure of **2**. For clarity, only the hydrogens on hydroxyl of Schiff base ligands are shown. Other hydrogens are omitted. The dinuclear unit is highlighted with black bonds. Cu, sky-blue; O, red; N, blue; C, gray; H, white (see http://dx.doi.org/10.1080/00958972.2013.876625 for color version).

Table 1. Crystallographic data and structure refinement parameters for **1–4**.

Compounds	**1**	**2**	**3**	**4**
Formulas	$C_{24}H_{34}Co_2N_3O_{11}$	$C_{26}H_{36}Cu_2N_2O_9$	$C_{52}H_{74}Cu_4N_4O_{15}$	$C_{46}H_{74}Mn_3N_2O_{22}$
Crystal system	Orthorhombic	Triclinic	Triclinic	Monoclinic
Space group	*Pna21*	*P-1*	*P-1*	$P2_1/c$
Formula weight	658.41	647.65	1249.36	1171.89
a, Å	10.104(3)	8.7530(11)	13.0373(13)	9.5347(7)
b, Å	18.588(5)	11.6346(14)	15.0722(15)	9.7892(8)
c, Å	14.367(4)	15.0184(18)	15.9924(16)	29.018(2)
α, °	90	100.0240(10)	64.0790(10)	90
β, °	90	94.5920(10)	85.834(2)	92.3990(10)
γ, °	90	111.163(2)	85.967(2)	90
V, Å^3	2698.3(13)	1387.4(3)	2816.3(5)	2706.1(4)
Z	4	2	2	2
T, K	298(2)	298(2)	298(2)	298(2)
λ, Å	0.71073	0.71073	0.71073	0.71073
ρ, g cm^{-3}	1.621	1.550	1.473	1.438
Reflections collected	10,998	7316	14,085	13,270
Unique	4594	4834	9748	4779
R_{int}	0.0608	0.0286	0.0438	0.0485
R_1 [$I > 2\sigma(I)$][a], R_1 (all data)[a]	0.0494, 0.0722	0.0430, 0.0641	0.0708, 0.1341	0.0694, 0.1163
wR_2 [$I > 2\sigma(I)$], wR_2 (all data)	0.1195, 0.1367	0.1051, 0.1134	0.1740, 0.2273	0.1856, 0.2342

[a] $R = \sum (|F_o - F_c|)/\sum |F_o| \cdot wR = \{\sum [w(|F_o - F_c|)^2]/\sum [w|F_o|^2]\}^{1/2}$.

Table 2. Selected bond lengths (Å) and angles (°) for **1–4**.

1			
Co(1)–O(6)	2.027(4)	Co(1)–O(5)	2.145(4)
Co(1)–O(2)	2.058(4)	Co(2)–O(2)	1.896(4)
Co(1)–O(3)	2.110(4)	Co(2)–O(6)	1.892(4)
O(6)–Co(1)–O(2)	78.7(2)	O(6)–Co(2)–O(2)	86.2(2)
Co(2)–O(2)–Co(1)	97.0(2)	Co(2)–O(6)–Co(1)	98.1(2)
O(3)–Co(1)–O(5)	176.2(2)	N(1)–Co(2)–N(2)	173.7(2)
2			
Cu(1)–O(2)	1.957(2)	Cu(1)–O(4)	1.987(2)
Cu(2)–O(2)	2.316(2)	Cu(2)–O(5)	1.966(2)
O(2)–Cu(1)–N(1)	84.58(9)	O(1)–Cu(1)–N(1)	94.03(9)
O(2)–Cu(1)–O(4)	93.60(8)	O(5)–Cu(2)–O(2)	89.54(8)
3			
Cu(1)–O(2)	1.925(5)	Cu(3)–O(2)	2.781(5)
Cu(1)–O(5)	1.961(5)	Cu(3)–O(8)	1.941(5)
Cu(1)–O(8)	2.594(5)	Cu(3)–O(11)	1.946(5)
Cu(2)–O(5)	1.934(5)	Cu(3)–O(13)	2.564(6)
Cu(2)–O(8)	1.950(5)	Cu(4)–O(2)	1.954(6)
Cu(2)–O(11)	2.722(5)	Cu(4)–O(5)	2.558(6)
Cu(4)–O(11)	1.912(5)		
O(8)–Cu(1)–O(2)	81.5(2)	O(5)–Cu(2)–O(8)	88.9(2)
O(8)–Cu(3)–O(11)	90.6(2)	O(10)–Cu(4)–O(2)	94.0(2)
4			
Mn(1)–O(2)	1.875(4)	Mn(2)–O(2)	2.142(4)
Mn(1)–O(5)	1.961(5)	Mn(2)–O(8)	2.165(5)
Mn(1)–O(4)	2.286(5)	Mn(2)–O(6)	2.222(4)
Mn(1)–O(7)	2.205(5)		
O(7)–Mn(1)–O(4)	175.0(2)	O(2)–Mn(2)–O(8)	92.2(2)
Mn(1)–O(2)–Mn(2)	121.3(2)	O(2)–Mn(2)–O(6)	88.4(2)

Table 3. Hydrogen bonding geometries for **1–4** [(Å) and (°)].

Compound	D–H···A	d(H···A)	d(D···A)	∠(DHA)	Symmetry codes
1	O(7)–H(7B)···O(4)#1	1.97	2.814(6)	172.3	#1: $-x+1$, $-y+2$, $z+1/2$; #2: $x-1/2$,
	O(7)–H(7C)···O(10)#2	2.02	2.866(6)	173.0	$-y+3/2$, z
	O(5)–H(5A)···O(11)	1.95	2.765(6)	177.6	
2	O(7)–H(7)···O(2)#2	1.66	2.474(4)	174.0	#1: $-x+1$, $-y+1$, $-z+1$; #2: $x-1$, y, z;
	O(3)–H(3)···O(6)#2	1.98	2.803(4)	177.0	#3: $-x+1$, $-y+1$, $-z$
	C(16)–H(16)···O(8)#3	2.68	3.571(5)	160.0	
3	O(14)–H(14)···O(12)#1	2.22	3.01(2)	162.5	#1: $x+1$, y, z; #2: $-x+1$, $-y+2$, $-z+1$
	C(15)–H(15)···O(14)	2.47	3.36(2)	159.9	
	O(15)–H(15D)···O(6)	2.06	2.915(9)	179.8	
	O(9)–H(9)···O(15)#2	1.85	2.658(9)	168.2	
4	C(9)–H(9)···O(5)#1	2.63	3.486(8)	153.2	#1: $-x+1$, $y-1/2$, $-z+3/2$

Cu–O–Cu angle are 3.149(8) Å and 94.55(10)°, close to the distances observed for similar dinuclear copper compounds [24–27].

Additionally, the uncoordinated hydroxyl O(3) and phenolic O(6) participate in intermolecular H-bonding, resulting in a linear structure. The weak C(16)–H(16)···O(8) interaction is responsible for the packing into a sheet structure (figure S2).

3.2.3. Structure of $[Cu_4(HL^1)_4(C_2H_5OH)]\cdot C_2H_5OH\cdot H_2O$ (3). Compound **3** displays a tetranuclear structure. As shown in figure 3, the asymmetric unit is composed of four crystallographically independent Cu ions, four $(HL^1)^{2-}$, one coordinated ethanol, one free ethanol, and one water. Coppers possess two different coordination environments. Cu(1), Cu(2), and Cu(4) are five-coordinate with distorted square-pyramidal geometry (τ(Cu(1)) = 0.182, τ(Cu(2)) = 0.100, and τ(Cu(4)) = 0.158), respectively. The basal plane of each square pyramid is occupied by imine nitrogen and one phenolic oxygen, and hydroxyl oxygen of one $(HL_1)^{2-}$ and one hydroxyl of the other Schiff base. The axial position is occupied by hydroxyl oxygen of the third Schiff base ligand. Cu(3) is six-coordinate and exhibits a distorted tetragonal bipyramid. The equatorial plane is composed of imine nitrogen and one phenolic oxygen, and hydroxyl oxygen of one $(HL_1)^{2-}$ and one hydroxyl of another Schiff base liand. The hydroxyl oxygen of the third Schiff base ligand and one ethanol are situated at apical positions.

All coordination spheres are distorted. Cu–O and Cu–N bonds in the equatorial planes and along the axes are 1.900(4)–1.950(4) and 2.564(5)–2.722(4) Å due to the Jahn–Teller effect. Mean deviations of donors from the plane for these centers are 0.189(2), 0.126(2), 0.106(3), and 0.217(2) Å, respectively. The copper centers deviate from the least-squares planes by 0.078(3), 0.034(3), 0.024(3), and –0.075(3) Å, respectively.

As a result, four Cu centers are connected by four Schiff base ligands $(\mathbf{HL}^1)^{2-}$ in μ_3-$\eta^1:\eta^1:\eta^3:\eta^0$ fashion (scheme 2d), resulting in a $\{Cu_4(\mu_3\text{-}O)_4\}$ cubane-like structure in which four coppers and four terminal hydroxyls occupy alternating corners [28]. The Cu···Cu distances and Cu–O–Cu angles are 3.167(1)–3.591(1) Å and 67.82(15)–99.20(17)°, indicating that the cubane is much distorted.

The cubane moieties interact with each other through hydrogen bonding interactions between C(15), uncoordinated ethanol O(14) and O(12) of free hydroxyl [O(14)–H(14)···O(12) and C(15)–H(15)···O(14)] to form a one-dimensional chain along the *c* axis. The formation of sheet structure occurs through hydrogen bonding interactions between free water O(15) and two oxygens [O(6) and O(9)] of uncoordinated hydroxyl groups (figure S3).

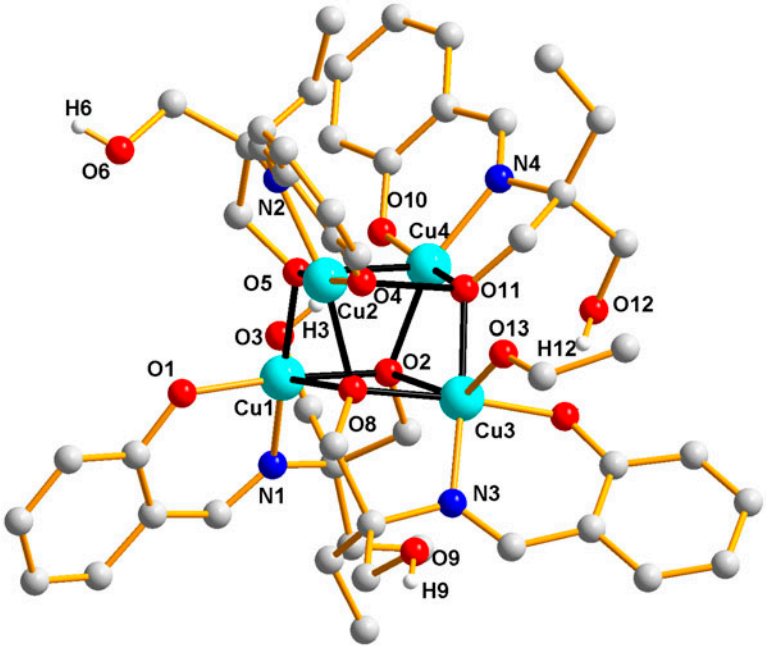

Figure 3. View of the molecular structure of **3**. For clarity, only the hydrogens on hydroxyl of Schiff base ligands are shown. Other hydrogens are omitted. The tetranuclear unit is highlighted with black bonds. Cu, sky-blue; O, red; N, blue; C, gray; H, white (see http://dx.doi.org/10.1080/00958972.2013.876625 for color version).

3.2.4. Structure of $[Mn_3(HL^2)_2(CH_3OH)_2(CH_3COO)_4]\cdot 2(CH_3OH)\cdot H_2O$ (4). Compound **4** possesses a mixed-valence trinuclear structure. Three linear Mn ions are found within the trinuclear crystal structure [29]. The central Mn(2) is located on a crystallographic inversion center and flanked by symmetry-related peripheral Mn ions [Mn(1) and Mn(1A)] (figure 4). Mn(1) resides in a [NO_5] distorted octahedral environment formed by N(1), O(1), and O(2) of the tetradentate Schiff base ligand and O(5) of acetate bridges with one oxygen from a neutral oxygen donor ligand. The bond lengths are 1.875(4)–2.286(5) Å. Mn(1) deviates 0.084(3) Å from the least-square plane through O(1), N(1), O(2), and O(5), and the mean deviation of the donors from the plane is 0.034(2) Å. The central Mn(2) is also six-coordinated *trans*-octahedral environment furnished by four oxygens of *syn–syn* bridging acetates in the least-square plane and two μ_2-hydroxyl oxygens.

Two deprotonated $(HL_2)^{2-}$ exhibit μ_2-$\eta^1:\eta^1:\eta^2:\eta^0$ coordination (scheme 2e) and cooperate with two *syn–syn* acetate groups, connecting three Mn centers to form a trinuclear $\{Mn_3(\mu_2\text{-}O)_2(\eta^2\text{-}COO)_2\}$ structure. Similar structures have been observed in $\{[(NiL)(n\text{-}BuOH)]_2(\mu\text{-}OAc)_2Ni\}\cdot n\text{-}BuOH$ (H_2L = 5,5'-dimethoxy-2,2'[(ethylene)dioxybis(nitrilomethylidyne)]diphenol) [30]. The peripheral and center Mn ions are +3 and +2, respectively, based on bond valence sum calculations [7]. The distance of Mn(1)···Mn(2) is 3.504(1) Å and the bridging angle of Mn(1)–O(alkoxide)–Mn(2) is 121.3(2)°.

In the crystal packing, the sheet structure is obtained through weak hydrogen bond interaction C(9)–H(9)···O(5) (figure S4).

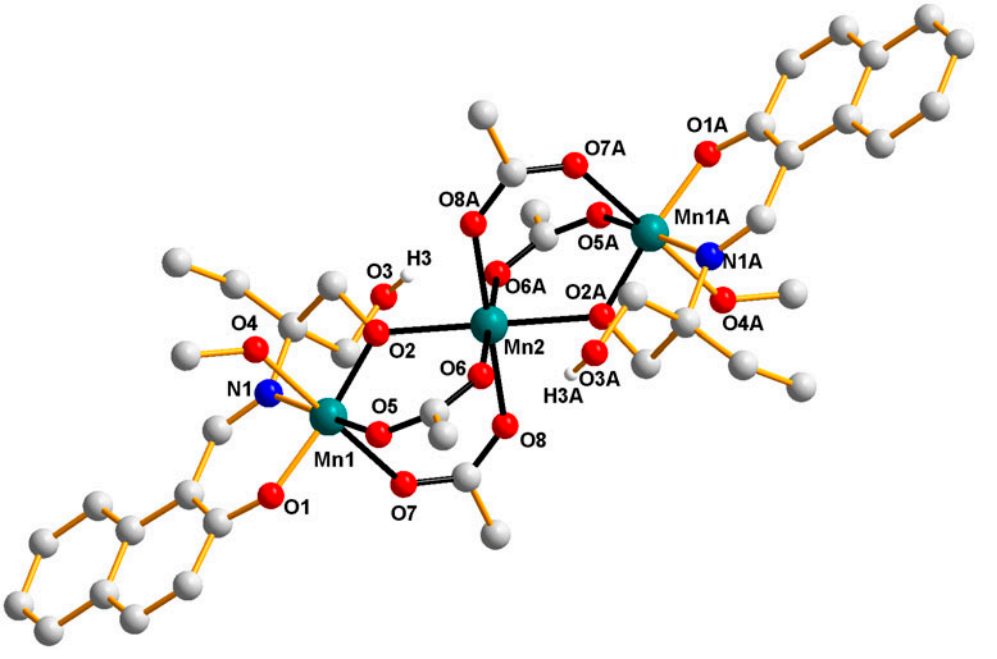

Figure 4. View of the molecular structure of **4**. For clarity, only the hydrogens on hydroxyl of Schiff base ligands are shown. Other hydrogens are omitted. The dinuclear unit is highlighted with bonds. Mn, dark green; O, red; N, blue; C, gray; H, white. Symmetry code: A, $-x+1$, $-y+1$, $-z+1$ (see http://dx.doi.org/10.1080/00958972.2013.876625 for color version).

3.3. *Discussion of structures*

The four compounds obtained from the reaction of metal salts with two different OH-rich Schiff base ligands exhibit diverse multinuclear structures including $\{Co_2(\mu_2\text{-}O)_2\}$, $\{Cu_2(\mu_2\text{-}O)(\eta^2\text{-}COO)\}$, $\{Cu_4(\mu_3\text{-}O)_4\}$, and $\{Mn_3(\mu_2\text{-}O)_2(\eta^2\text{-}COO)_2\}$. The phenomenon is influenced by several factors, such as coordination geometries of the metal centers, coordination modes of the Schiff base ligands, ratio of metal to ligand, nature of the counter ions, etc. As shown in scheme 2, two Schiff base ligands exhibit four different coordination modes in these compounds. Terminal hydroxyl oxygen could act as η^1-, η^2-, and η^3-bridges to connect metal centers. Additionally, both Schiff base ligands are flexible with respect to the relative orientations of the N–C bonds connecting C=N and $-(CH_2CH_2OH)_2(CH_2CH_3)$ groups. As a result, many conformations of these ligands are formed according to the requirement of the metal centers. A superimposed picture of the ligands put this into perspective as shown in figure 5.

Except for **1**, the other compounds possess free hydroxyl groups involved in the formation of intra- and intermolecular hydrogen bonds. Other small moieties including water (**1**), ethanol (**3**), and acetate (*syn–syn* fashion, **2** and **4**) furnish the coordination sphere of the metal ions in addition to the donors of the Schiff base ligands.

3.4. *XRD patterns and TGA studies*

The experimental XRD patterns agreed well with the simulated ones generated on the basis of single-crystal analyses for **1–4** (figure S5), suggesting the phase purity of the products.

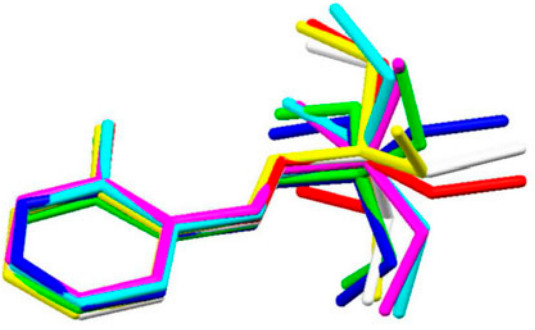

Figure 5. Overlay of two Schiff base moieties in the four compounds.

The thermal stabilities of **1–4** were investigated using TGA (figure S6). For **1**, three consecutive decompositions are attributed to the gradual release of the Schiff base ligands, leading to the formation of cobalt oxide as the residue. The TGA curve of **2** shows gradual weight loss from 99 to 144 °C, corresponding to the loss of free water (found 2.97%, Calcd 2.78%); the second weight loss from 124 to 165 °C corresponds to loss of acetate with mass loss of 9.38% (Calcd 9.11%); and the third weight loss at 250–290 °C with 50.1% (Calcd 68.9%) corresponds to loss of Schiff base. The residue is CuO [31]. For **3**, the first step of decomposition at 69–125 °C corresponds to loss of solvent molecules with 11.01% (Calcd 9.28%) mass loss, and then **3** decomposed continuously to 284 °C with 65.25% (Calcd 71.82%) corresponding to the gradual loss of Schiff base. The residue is CuO. For **4**, the first weight loss of 9.52% (Calcd 15.87%) below 92 °C is assigned to the liberation of the solvent. The second weight loss occurs at 150–244 °C, which is attributed to the elimination of acetate (found 17.69%, Calcd 20.13%). Then, **4** decomposed continuously to 534 °C with 35.52% (Calcd 46.65%) corresponding to loss of Schiff base. The residue is a mixture of MnO and Mn_2O_3.

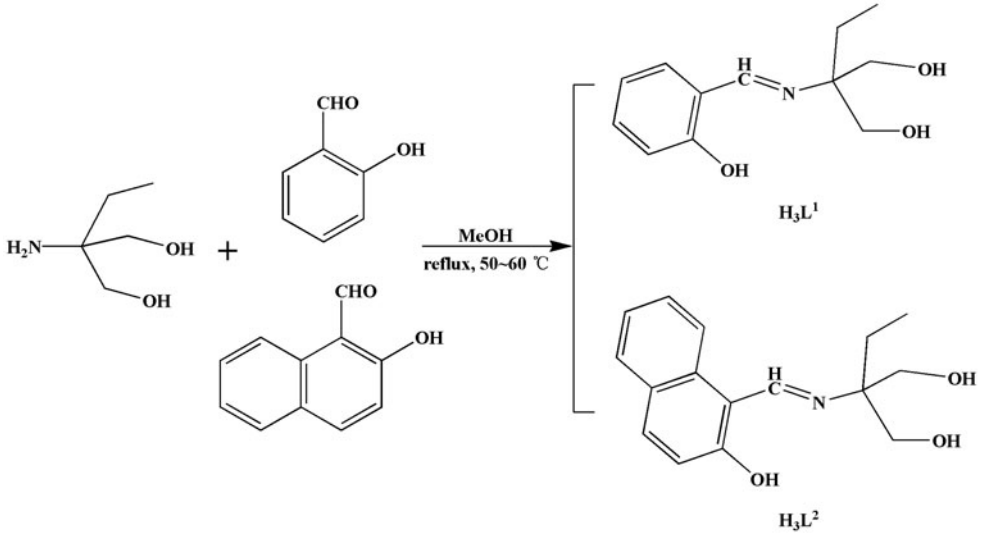

Scheme 1. The syntheses of $\mathbf{H_3L^1}$ and $\mathbf{H_3L^2}$.

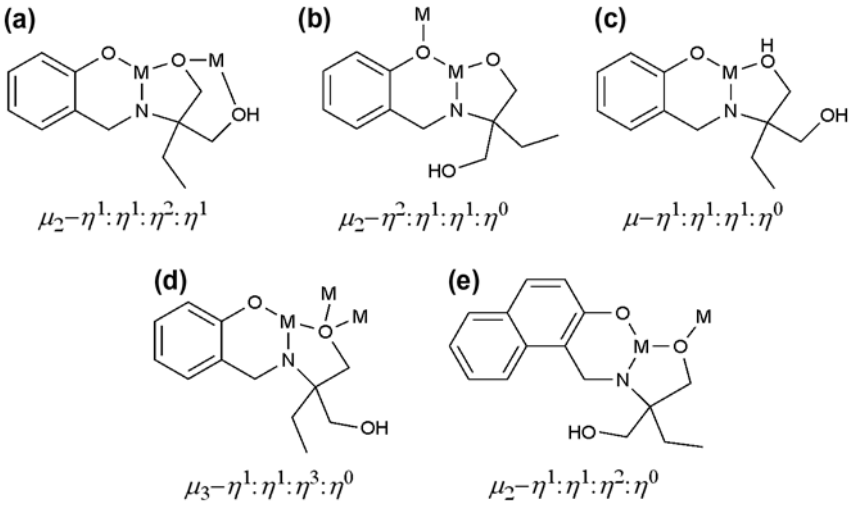

Scheme 2. The coordination modes of the Schiff base ligands.

3.5. *Magnetic properties*

Variable temperature magnetic susceptibility measurements (2–300 K) for **1–4** were measured on polycrystalline samples using a Quantum Design MPMS-XL 7 SQUID magnetometer with an applied magnetic field of 1 kOe.

The magnetic properties of **1** are attributed to one octahedrally coordinated Co(II), since the Co(III) site is diamagnetic. The $\chi_M T$ *versus* T plot of **1** is shown in figure S7(1). At 300 K, the experimental $\chi_M T$ value is 1.83 $cm^3\,KM^{-1}$, which is lower than that expected for a high-spin Co^{II} ion (1.87 $cm^3\,KM^{-1}$ with S = 3/2, g = 2.0) due to the occurrence of an unquenched orbital contribution typical of the $^4T_{1g}$ ground-state in octahedral high-spin Co^{II} complexes [32]. Upon cooling, $\chi_M T$ gradually decreases to a minimum of 0.83 $cm^3\,KM^{-1}$ at 42 K, resulting from the depopulation of the six-Kramers double state as a consequence of the combined effect of spin–orbit coupling and distortion from octahedral symmetry [33]. In fact, between 300 and 42 K, $\chi_M T$ is dominated by single ion magnetic behavior of uncoupled Co(II) ions. When the temperature continues to decrease from 42 K, $\chi_M T$ slowly increases to a maximum of 0.88 $cm^3\,KM^{-1}$ at 35 K, indicating intermolecular ferromagnetic interactions, typical for monomeric systems as expected with metal centers separated (8.189 Å) in **1**. Below 35 K, $\chi_M T$ goes down to 0.56 $cm^3\,KM^{-1}$ at 2 K, due to long-range interaction between the highly anisotropic spin carriers [34].

The $\chi_M T$ *versus* T plot of **2** is shown in figure S7(2). At 300 K, the $\chi_M T$ value is 0.79 $cm^3\,KM^{-1}$, slightly higher than that expected (0.75 $cm^3\,KM^{-1}$) for two isolated copper ions with S = 1/2 and g = 2 [35]. Upon cooling, $\chi_M T$ slowly increases to 0.84 $cm^3\,KM^{-1}$ at 78 K, followed by a pronounced drop to the minimum value of 0.098 $cm^3\,KM^{-1}$ at 2 K. This increase of $\chi_M T$ at 300–78 K represents a characteristic feature of intramolecular ferromagnetic interactions between Cu(II) ions. The decrease of $\chi_M T$ below 78 K is due to superposition with isolated copper ions orbital momentum [36].

The $\chi_M T$ *versus* T plot of **3** is shown in figure S7(3). The value of $\chi_M T$ at room temperature is 1.38 $cm^3\,KM^{-1}$, less than that expected for four magnetically isolated copper(II) ions

(1.50 $cm^3\,KM^{-1}$ supposed S = 1/2, g = 2). Upon cooling, the $\chi_M T$ gradually increases and reaches a maximum of 1.43 $cm^3\,KM^{-1}$ at about 100 K, and then rapidly falls to 0.29 $cm^3\,KM^{-1}$ at 2 K. The increase of $\chi_M T$ from 100 to 300 K upon cooling indicates the presence of weak ferromagnetic coupling. The decrease of $\chi_M T$ at low temperature shows that the magnetic interactions are dominated by an antiferromagnetic interaction among copper(II) clusters, resulting from μ_3-hydroxyl bridges.

The $\chi_M T$ *versus* T plot of **4** is shown in figure S7(4). At 300 K, the experimental $\chi_M T$ value is 9.51 $cm^3\,KM^{-1}$, slightly lower than the value of 10.37 $cm^3\,KM^{-1}$ for two Mn(III) ions and one high-spin Mn(II) ($S_{MnIII} = 2.0$, $S_{MnII} = 5/2$ and assuming $g_{MnII} = g_{MnIII} = 2.0$) [37, 13]. Upon cooling, the $\chi_M T$ value gradually decreases and reaches a minimum of 2.66 $cm^3\,KM^{-1}$ at 7 K, which reveals an antiferromagnetic coupling in **4**. However, with further cooling, $\chi_M T$ increases to a maximum of 4.66 $cm^3\,KM^{-1}$ at 3 K, followed by a drop to 4.03 $cm^3\,KM^{-1}$ at 2 K, possibly due to the effect of zero-field splitting arising from the Mn ions, or to a field-saturation effect, or to both factors [38].

3.6. *Antitumor activities*

Compounds **1–4** are screened for tumor-inhibiting activity *in vitro* against the K-562 and HL-60 cell lines. The corresponding inhibitory concentration IC_{50} values are listed in table 4. Experiments show that **1** is a more efficient antitumor agent for K-562 and its antitumor activity is also much higher than that of DDP [39] and CBP [40]. The others do not show antitumor activity to K-562, perhaps due to poor solubility that controls the rate of entry of molecules into the cell [41]. Against the HL-60 cell line, **2** exhibits more activity than CBP, but not as effective as DDP [42–44]. Generally, most chemical, physical, and biological functions of therapeutic agents are strongly dependent on their special structure. In contrast to DDP and CBP, **1–4** display novel spatial structures. The test results suggest that the structures probably contribute to their diverse biofunctions on tumor proliferation. Different model cell showing different activities suggest that susceptibility to compounds treatment is largely dependent on cell types.

The study provides insight into expanding multifunctional compounds. It is necessary to further investigate the antiproliferation mechanism of these agents and explore their applications. Slight modification based on present structures is expected to enhance anticancer ability and widen their spectrums to develop preclinical chemotherapeutic agents with high efficiency and low toxicity.

Table 4. Half maximal inhibitory concentration (μM) of **1–4** against leukemia cell lines.

	IC_{50} (μM)	
Compound	K-562	HL-60
1	5.46	>100
2	>100	9.83
3	>100	>100
4	>100	>100
DDP	9.30	2.13
CBP	49.7	23.24

4. Conclusion

Assembled from two OH-rich Schiff base ligands, four compounds have been synthesized and characterized. The terminal hydroxyl arm can freely twist, bend, and chelate/bridge the metals, yielding products with different nuclearities. Compound **1** possesses mixed-valence dinuclear Co_2O_2 with Co(II) and Co(III) ions linked through μ_2-hydroxyl. Compound **2** displays a binuclear Cu(II) structure containing a μ_2-hydroxyl oxygen and a single *syn–syn* acetate bridge. Compound **3** is a tetranuclear cube-shaped Cu(II) complex. Compound **4** is a linear trinuclear-manganese complex in which the terminal Mn(III) and the central Mn(II) are linked by a μ_2-hydroxyl oxygen and two *syn–syn* acetate bridges. More compounds of such Schiff base ligands are required to understand the coordination behaviors of the ligands [45] and factors that modulate the final structure (e.g. Mn^{III}–Cu^{II} heterometallic aggregates synthesized by reaction in organic solvents) [46]. Although the metal ions are mediated by the μ-hydroxyl, temperature-dependent magnetic susceptibility measurements reveal that the compounds exhibit diverse magnetic properties. Work concerning the magneto-structural correlation and the antitumor activities will be further investigated in our laboratory.

Supplementary material

Crystallographic data in CIF format have been deposited with the Cambridge Crystallographic Data Center, CCDC No. 899128 (**1**), 899130 (**2**), 899131 (**3**), 902447 (**4**). Copies of the data may be obtained free of charge on application to CCDC, 12 Union Road, Cambridge CB21EZ, UK (Fax: +44 1223 336033; E-mail: deposit@ccdc.cam.ac.uk or http://www.ccdc.cam.ac.uk).

Acknowledgments

This work was supported by the Natural Science Foundation of Shandong Province (ZR2010BQ021, 2011YD02093) and the Natural Science Foundation of China [grant number 20971063].

References

[1] A.D. Harley, G.J. Guskey, G.L. Geoffroy. *Organometallics*, **2**, 53 (1983).
[2] E.K. Brechin, C. Boskovic, W. Wernsdorfer, J. Yoo, A. Yamaguchi, E.C. Sañudo, T.R. Concolino, A.L. Rheingold, H. Ishimoto, D.N. Hendrickson, G. Christou. *J. Am. Chem. Soc.*, **124**, 9710 (2002).
[3] V.W. Yam, K.K. Lo. *Chem. Soc. Rev.*, **28**, 323 (1999).
[4] A. Ray, G. Pilet, C.J. Gómez-García, S. Mitra. *Polyhedron*, **28**, 511 (2009).
[5] C.M. da Silva, D.L. da Silva, L.V. Modolo, R.B. Alves, M.A. de Resende, C.V.B. Martins, Â. de Fátima. *J. Adv. Res.*, **2**, 1 (2011).
[6] S. Banerjee, M. Nandy, S. Sen, S. Mandal, G.M. Rosair, A.M.Z. Slawin, C.J.G. García, J.M. Clemente-Juan, E. Zangrando, N. Guidolin, S. Mitra. *Dalton Trans.*, **40**, 1652 (2011).
[7] D. Liu, Q. Zhou, Y. Chen, F. Yang, Y. Yu, Z. Shi, S. Feng. *Dalton Trans.*, **39**, 5504 (2010).
[8] S. Shit, G. Rosair, S. Mitra. *J. Mol. Struct.*, **991**, 79 (2011).
[9] D.P. Kessissoglou, X. Li, W.M. Butler, V.L. Pecoraro. *Inorg. Chem.*, **26**, 2487 (1987).
[10] S.S. Tandon, S.D. Bunge, N. Patel, L.K. Thompson. *Inorg. Chem. Commun.*, **12**, 1077 (2009).
[11] M. Nihei, N. Hoshino, T. Ito, H. Oshio. *Polyhedron*, **22**, 2359 (2003).

[12] L.-L. Hu, Z.-Q. Jia, J. Tao, R.-B. Huang, L.-S. Zheng. *Dalton Trans.*, **44**, 6113 (2008).
[13] N. Hoshino, T. Ito, M. Nihei, H. Oshio. *Inorg. Chem. Commun.*, **6**, 377 (2003).
[14] H. Xiang, Y. Lan, L. Jiang, W.-X. Zhang, C.E. Anson, T.-B. Lu, A.K. Powell. *Inorg. Chem. Commun.*, **16**, 51 (2012).
[15] C.P. Pradeep, P.S. Zacharias, S.K. Das. *Polyhedron*, **24**, 1410 (2005).
[16] H.-H. Li, M.-J. Niu, D.-W. Sun, S.-N. Wang, S. Cheng. *Inorg. Chem. Commun.*, **27**, 97 (2013).
[17] M. Belicchi-Ferrari, F. Bisceglie, C. Cavalieri, G. Pelosi, P. Tarasconi. *Polyhedron*, **26**, 3774 (2007).
[18] D.S. Nesterov, V.G. Makhankova, V.N. Kokozay, B.W. Skelton. *Inorg. Chim. Acta*, **358**, 4519 (2005).
[19] G.M. Sheldrick. *Acta Crystallogr. Sect. A Found. Crystallogr.*, **64**, 112 (2008).
[20] T. Mosmann. *J. Immunol. Methods*, **65**, 55 (1983).
[21] M. Koikawa, M. Ohba, T. Tokii. *Polyhedron*, **24**, 2257 (2005).
[22] R. Bikas, H.H. Monfared, T. Lis, M. Siczek. *Inorg. Chem. Commun.*, **15**, 151 (2012).
[23] A.W. Addison, T.N. Rao, J. Reedijk, J. van Rijn, G.C. Verschoor. *J. Chem. Soc., Dalton Trans.*, **7**, 1349 (1984).
[24] H.-Y. Zhao, X.-H. Qiu, X.-L. Tong, P.-W. Shen. *Chin. J. Struct. Chem.*, **25**, 1095 (2006).
[25] M.-X. Dong, L.-Y. Zhong, M. Zhang. *J. Coord. Chem.*, **64**, 3265 (2011).
[26] F.-H. Zeng, J. Ni, C.-X. Ding, Y.-S. Xie. *J. Coord. Chem.*, **65**, 2247 (2012).
[27] L.-J. Lu, Y.-Y. Song, H. Liu, J.-Y. Zhang. *J. Coord. Chem.*, **65**, 1278 (2012).
[28] H. Arora, F. Lloret, R. Mukherjee. *Inorg. Chem.*, **48**, 1158 (2009).
[29] V. Tangoulis, D.A. Malamatari, G.A. Spyroulias, C.P. Raptopoulou, A. Terzis, D.P. Kessissoglou. *Inorg. Chem.*, **39**, 2621 (2000); D.P. Kessissoglou, X. Li, W.M. Butler, V.L. Pecoraro. *Inorg. Chem.*, **26**, 2487 (1987); X. Li, D.P. Kessissoglou, M.L. Kirk, C.J. Bender, V.L. Pecoraro. *Inorg. Chem.*, **27**, 3 (1988); D.P. Kessissoglou, M.L. Kirk, M.S. Lah, X. Li. *Inorg. Chem.*, **31**, 5424 (1992); D.A. Malamatari, P. Hitou, A.G. Hatzidimitriou, F.E. Inscore, A. Gourdon, M.L. Kirk, D.P. Kessissoglou. *Inorg. Chem.*, **34**, 2493 (1995); V. Tangoulis, D.A. Malamatari, K. Soulti, V. Stergiou, C.P. Raptopoulou, A. Terzis, T.A. Kabanos, D.P. Kessissoglou. *Inorg. Chem.*, **35**, 4974 (1996).
[30] W.-K. Dong, Y.-X. Sun, L. Li. *J. Coord. Chem.*, **65**, 2332 (2012).
[31] S.A. Patil, S.N. Unki, A.D. Kulkarni. *J. Mol. Struct.*, **985**, 330 (2011).
[32] C.-M. Liu, Y. Song, D.-Q. Zhang. *Inorg. Chem. Commun.*, **13**, 160 (2010).
[33] S.-N. Wang, J.-F. Bai, H. Xing, Y. Li, Y. Song, Y. Pan, M. Scheer, X. You. *Cryst. Growth Des.*, **7**, 747 (2007).
[34] T. Jurca, A. Farghal, P.-H. Lin, I. Korobkov, M. Murugesu, D.S. Richeson. *J. Am. Chem. Soc.*, **133**, 15814 (2011); F. Lloret, M. Julve, J. Cano, R. Ruiz-García, E. Pardo. *Inorg. Chim. Acta*, **361**, 3432 (2008).
[35] A.M. Greenaway, C.J. O'Connor, J.W. Overman, E. Sinn. *Inorg. Chem.*, **20**, 1508 (1981).
[36] I.C. Lazzarini, L. Carrella, E. Rentschler, P. Alborés. *Polyhedron*, **31**, 779 (2012).
[37] Y.-G. Li, Q. Wu, L. Lecren. *J. Mol. Struct.*, **890**, 339 (2008).
[38] M. Yuan, F. Zhao, W. Zhang, F. Pan, Z.-M. Wang, S. Gao. *Chem. Eur. J.*, **13**, 2937 (2007).
[39] P.-L. Qian, J. Zhu, Z.-Y. Liu. *J. Chin. Clin. Med.*, **137**, 14795 (2005).
[40] Q.-H. Dong, S. Zheng, Q.-H. Lu. *Chin. J. Oncol.*, **17**, 24 (2002).
[41] M.S. Nair, D. Arish, R.S. Joseyphus. *J. Saudi Chem. Soc.*, **16**, 83 (2012).
[42] E.T. Martins, H. Baruah, J. Kramarczyk, G. Saluta, C.S. Day, G.L. Kucera, U. Bierbach. *J. Med. Chem.*, **44**, 4492 (2001).
[43] A.I. de Vos, K. Nooter, J. Verweij, W.J. Loos, E. Brouwer, P. de Bruijn, E.J. Ruijgrok, M.E. van der Burg, G. Stoter, A. Sparreboom. *Ann. Oncol.*, **8**, 1145 (1997).
[44] Y.-E. Kwon, K.-J. Whang, Y.-J. Park, K.H. Kim. *Bioorg. Med. Chem.*, **11**, 1669 (2003).
[45] Y.-F. Chen, L. Wei, J.-L. Bai, H. Zhou. *J. Coord. Chem.*, **64**, 1153 (2011).
[46] Q. Wu, Q. Shi, Y.-G. Li, E.-B. Wang. *J. Coord. Chem.*, **61**, 3080 (2011).